CORA Cork Open Research Archive
Cartlann Taighde Oscailte Chorcaí

UCC Library and UCC researchers have made this item openly available. Please let us know how this has helped you. Thanks!

Title	Theory of hole mobility in strained Ge and III-V p-channel inversion layers with high-kappa insulators
Author(s)	Zhang, Yan; Fischetti, Massimo V.; Soree, B.; O'Regan, Terrance P.
Publication date	2010
Original citation	Zhang, Y., Fischetti, M. V., Sorée, B. and O'Regan, T. (2010) 'Theory of hole mobility in strained Ge and III-V p-channel inversion layers with high-κ insulators', Journal of Applied Physics, 108(12), 123713 (9pp). doi: 10.1063/1.3524569
Type of publication	Article (peer-reviewed)
Link to publisher's version	http://aip.scitation.org/doi/10.1063/1.3524569 http://dx.doi.org/10.1063/1.3524569 Access to the full text of the published version may require a subscription.
Rights	**© 2010, American Institute of Physics. This article may be downloaded for personal use only. Any other use requires prior permission of the author and AIP Publishing. The following article appeared in Zhang, Y., Fischetti, M. V., Sorée, B. and O'Regan, T. (2010) 'Theory of hole mobility in strained Ge and III-V p-channel inversion layers with high-κ insulators', Journal of Applied Physics, 108(12), 123713 (9pp). doi: 10.1063/1.3524569 and may be found at http://aip.scitation.org/doi/10.1063/1.3524569**
Item downloaded from	http://hdl.handle.net/10468/4741

Downloaded on 2021-01-27T10:07:16Z

UCC University College Cork, Ireland
Coláiste na hOllscoile Corcaigh

Theory of hole mobility in strained Ge and III-V p-channel inversion layers with high-κ insulators

Yan Zhang, M. V. Fischetti', B. Sorée, and T. O'Regan

Citation: Journal of Applied Physics **108**, 123713 (2010); doi: 10.1063/1.3524569
View online: http://dx.doi.org/10.1063/1.3524569
View Table of Contents: http://aip.scitation.org/toc/jap/108/12
Published by the American Institute of Physics

Articles you may be interested in

Band structure, deformation potentials, and carrier mobility in strained Si, Ge, and SiGe alloys
Journal of Applied Physics **80**, 2234 (1998); 10.1063/1.363052

Theory of hole mobility in strained Ge and III-V p-channel inversion layers with high-κ insulators

Yan Zhang,[1] M. V. Fischetti,[1,a)] B. Sorée,[2] and T. O'Regan[3]
[1]*Department of Electrical and Computer Engineering, University of Massachusetts, Amherst, Massachusetts 01003, USA*
[2]*IMEC, Kapeldreef 75, B-3001 Leuven, Belgium*
[3]*Tyndall National Institute, University College, Cork, Ireland*

(Received 31 August 2010; accepted 26 October 2010; published online 29 December 2010)

We present a comprehensive investigation of the low-field hole mobility in strained Ge and III-V (GaAs, GaSb, InSb, and $In_{1-x}Ga_xAs$) p-channel inversion layers with both SiO_2 and high-κ insulators. The valence (sub)band structure of Ge and III-V channels, relaxed and under biaxial strain (tensile and compressive) is calculated using an efficient self-consistent method based on the six-band $\mathbf{k}\cdot\mathbf{p}$ perturbation theory. The hole mobility is then computed using the Kubo–Greenwood formalism accounting for nonpolar hole-phonon scattering (acoustic and optical), surface roughness scattering, polar phonon scattering (III-Vs only), alloy scattering (alloys only) and remote phonon scattering, accounting for multisubband dielectric screening. As expected, we find that Ge and III-V semiconductors exhibit a mobility significantly larger than the "universal" Si mobility. This is true for MOS systems with either SiO_2 or high-κ insulators, although the latter ones are found to degrade the hole mobility compared to SiO_2 due to scattering with interfacial optical phonons. In addition, III-Vs are more sensitive to the interfacial optical phonons than Ge due to the existence of the substrate polar phonons. Strain—especially biaxial tensile stress for Ge and biaxial compressive stress for III-Vs (except for GaAs)—is found to have a significant beneficial effect with both SiO_2 and HfO_2. Among strained p-channels, InSb exhibits the largest mobility enhancement. $In_{0.7}Ga_{0.3}As$ also exhibits an increased hole mobility compared to Si, although the enhancement is not as large. Finally, our theoretical results are favorably compared with available experimental data for a relaxed Ge p-channel with a HfO_2 insulator. © *2010 American Institute of Physics*.
[doi:10.1063/1.3524569]

I. INTRODUCTION

Continued scaling of the physical size of conventional VLSI devices causes significant degradation of channel mobility (mainly because of Coulomb interactions[1–3] and increased scattering with interfacial roughness) as well as severe gate leakage problem. Several ideas aimed at retaining the much needed device performance (e.g., replacing Si with high-mobility channel materials, straining the channel, employing high dielectric-constant insulators) are either already in production or at an exploratory stage. In particular, attention has been paid to Ge and III-Vs as possible alternative channel materials: their intrinsic carrier mobility significantly higher than Si (for either electrons or holes)[4] promises high performance, while the advent of new gate-insulator materials—such as SiO_2 on a thin Si cap, GeO_xN_y and HfO_2—has rendered the prospect of a Ge or III-V technology more realistic.[5–8] Previous work has mainly focused either on electron mobility in Ge and III-V nMOS devices[9] or on hole mobility, but limited to Si p-channel inversion layers.[10–15] Recent theoretical work has dealt with the hole mobility in SiGe pMOS[11,16] and with the strain-dependent hole mobility, but limited to Ge p-channels and to the case of SiO_2 insulator.[17] However, little has been done theoretically for the more general cases of Ge and III-V p-channels with high-κ insulators.[14] This paper attempts to remedy this situation. As it is customary, we focus here on the hole mobility. While the low-field mobility may provide little information about the on-current performance of nanometer-scale devices,[18] however, it provides a more accurate comparison to experimental data, thus enabling us to understand the physics of the band structure and of the scattering process affecting these new structures. In addition, during a switching cycle devices spend a significant fraction of the total switching time operating in the linear regime, where the bona-fide low-field mobility controls their behavior. Thus, when taken with these considerations in mind, the low-field mobility represents an interesting quantity to focus on.

Hole mobility studies are complicated by the nonparabolic, warped, and anisotropic nature of the valence subband structure. Two are the main problems we need to face: obtain efficiently an accurate valence subband structure and employ physically accurate models to calculate the relaxation rates due to the various scattering processes which affect hole transport.

Regarding the first problem, previous work has pointed out the failure of effective mass[12] and of triangular-well approximation in strong inversion.[12,19] Methods based on simplifying expansions of the wave functions into suitable basis-functions,[20] or resorting to "brute force" and paying a hefty computational price[11] or unpredictable efficiency depending on the complexity of subband structures[19,21] have

a)Electronic mail: fischett@ecs.umass.edu.

 © 2010 American Institute of Physics

emphasized the need for an efficient and accurate computational method. We have previously presented[17] such a method which is still based on the by-now "usual" framework of the six-band $\mathbf{k}\cdot\mathbf{p}$ perturbation theory,[22,23] but extending the method introduced in Ref. 21: Having discretized the two-dimensional (2D) **K**-space with a coarse mesh, the subband energies and squared wave functions on this mesh are tabulated and a one-dimensional cubic-spline interpolation is employed to obtain the desired quantities at an arbitrary **K** point in the 2D Brillouin Zone.

The second problem we must face consists in calculating in a physically accurate way the various scattering mechanisms affecting hole transport in inversion layers. For nonpolar phonon (NP) scattering, we employ the very same model of Refs. 10, 13, 16, and 17 assuming once more equipartition, elastic scattering with nonpolar phonons, and making use of the isotropic approximation. Regarding scattering with surface roughness, we employ the full Ando's model for which a thorough discussion can be found in Refs. 10, 17, and 24–26. For the III-V compound semiconductors considered in this paper, the Frölich polar scattering with longitudinal optical (LO) phonons[27,28] is also taken into account. Furthermore, scattering due to the remote phonons or surface optical (SO) phonons originating from the dipole field of insulators (including the Landau damping of the coupled interfacial plasma modes) is also included to account for the effect of high-κ dielectrics.[29–31] Dielectric screening of the surface roughness potential, usually either neglected or treated in a simplified way using a simple scalar screening wave vector,[32] has been included employing a static, wave vector dependent multisubband screening model.[10,30,33,34] Due to the dynamic property of the LO phonon scattering potential, in this case dielectric screening should be treated in its full dynamic formulation.[34] Usually, however, simpler models are used: Either a static approximation[34] or the even more drastic use of an "effective screening parameter,"[32] strictly valid only in the electric quantum limit for a δ-function sheet charge distribution. In our calculations we treat dielectric screening of the LO-phonon scattering potential in the similar way as for SR scattering. A discussion of the effect of the various screening models will be given in a later section. NP scattering with acoustic and optical phonons is left intentionally unscreened, for the reasons discussed in Ref. 34. Coulomb scattering with interface traps, oxide charges, or ionized impurities (dopants) is neglected here since it only plays an important role in weak inversion case and we are interested in the best-scenario "intrinsic" mobility.

This paper is organized as follows: In Sec. II we briefly review the self-consistent $\mathbf{k}\cdot\mathbf{p}$/Poisson method. In Sec. III we discuss the physical models employed to treat the scattering processes and dielectric screening and in Sec. IV we present our results and a brief discussion. Conclusions are finally drawn in Sec. V.

II. SELF-CONSISTENT CALCULATION OF THE VALENCE SUBBAND STRUCTURE

In this section we present the method we have used to calculate the self-consistent valence subband structure.

Following the discussion in Ref. 17, we start with the six-band $\mathbf{k}\cdot\mathbf{p}$ eigenvalue problem which provides a sufficiently accurate hole dispersion for wave vectors close to the Γ symmetry point, namely, $k<0.3(2\pi/a_0)$, where a_0 is the lattice constant.[13] The Schrödinger-type equation we must solve is given by

$$[\hat{H}_{\mathbf{k}\cdot\mathbf{p}}+\hat{H}_{so}+\hat{H}_{\text{strain}}+\hat{I}eV(z)]\Psi_{\mathbf{K}}(z)=E(\mathbf{K})\Psi_{\mathbf{K}}(z). \quad (1)$$

Here the $\mathbf{k}\cdot\mathbf{p}$ Hamiltonian $\hat{H}_{\mathbf{k}\cdot\mathbf{p}}$, the spin-orbit Hamiltonian $\hat{H}_{so}$, and strain Hamiltonian $\hat{H}_{\text{strain}}$ have the same forms given in Refs. 10 and 17. The discretization of the 2D Brillouin Zone has been performed as described in Ref. 17 using a number $N_k=49$ of radial mesh points and a number $N_\phi=10$ of angular mesh points. All of the band structure parameters, the $\mathbf{k}\cdot\mathbf{p}$ Kohn–Luttinger parameters, the spin-orbit split-off energy Δ_{so}, and the deformation potential parameters for the strain Hamiltonian are taken from Ref. 35. We have assumed that the z-axis is perpendicular to the insulator/substrate interface and in Eq. (1) k_z must be interpreted as standing for $-i(d/dz)$. A nonuniform finite difference algorithm is employed to numerically solve this eigenvalue problem. The boundary conditions for the wave functions are set to be zero at insulator/substrate interface and at a distance sufficiently large from the interface (22 nm). We use the Broyden second method to accelerate the iteration employed to solve the coupled Schrödinger-type and Poisson equations.

III. PHYSICAL MODELS FOR HOLE MOBILITY IN AN INVERSION LAYER

In order to evaluate the mobility tensor we have followed Refs. 10 and 17, expressing the x-component of the momentum relaxation rate $\tau_x^{(\nu)}(K,\phi)$ accounting for the contributions from the scattering processes as

$$\frac{1}{\tau_x^{(\nu)}}=\frac{1}{\tau_{x,NP}^{(\nu)}}+\frac{1}{\tau_{x,SR}^{(\nu)}}+\frac{1}{\tau_{x,SO}^{(\nu)}}+\frac{1}{\tau_{x,LO}^{(\nu)}}+\frac{1}{\tau_{x,AL}^{(\nu)}}, \quad (2)$$

where $\tau_{x,NP}$, $\tau_{x,SR}$, $\tau_{x,SO}$, $\tau_{x,LO}$, and $\tau_{x,AL}$ are the momentum relaxation time for nonpolar acoustic/optical phonon scattering, surface roughness scattering, remote phonon scattering, LO phonon scattering (for polar materials only), and alloy scattering (for alloys only), respectively.

According to Refs. 10 and 30, the momentum relaxation rate is given by

$$\frac{1}{\tau_{\mu\nu}(\mathbf{K})}=\frac{2\pi}{\hbar}\int\frac{d\mathbf{K}'}{(2\pi)^2}|M_{\mu\mathbf{K}',\nu\mathbf{K}}|^2\delta[E_\mu(\mathbf{K})-E_\nu(\mathbf{K}')\pm\hbar\omega_{\mathbf{K}'-\mathbf{K}}]\times\frac{1-f(E')}{1-f(E)}\times\left\{1-\frac{v_x^{(\nu)(\mathbf{K}')}\tau_x^{(\nu)(\mathbf{K}')}f_x^{(\nu)(\mathbf{K}')}}{v_x^{(\mu)(\mathbf{K})}\tau_x^{(\mu)(\mathbf{K})}f_x^{(\mu)(\mathbf{K})}}\right\}, \quad (3)$$

where E' is the energy of the final state $\mathbf{K}'$ and $v_x^{(\mu)}(\mathbf{K})$ is x-component of the hole group velocity at the wave vector $\mathbf{K}$ and $M_{\mu\mathbf{K}',\nu\mathbf{K}}$ is the scattering potential $\Phi(\mathbf{R},z)$ associated matrix element defined by

$$M_{\mu\mathbf{K}',\nu\mathbf{K}} = \int \frac{d\mathbf{R}}{(2\pi)^2} e^{-i(\mathbf{K}'-\mathbf{K})\cdot\mathbf{R}} \times \int_0^\infty dz \Psi_{\mathbf{K}'}^{(\nu)\dagger}(z) \cdot \Psi_{\mathbf{K}}^{(\mu)} \times (z)\Phi(\mathbf{R},z). \quad (4)$$

The implicit expression given by Eq. (3) requires a self-consistent solution since the total relaxation rate appears inside the integral, rendering the problem equivalent to finding the solution of a nonlinear integral equation. For the isotropic and elastic NP scattering, the term in curly brackets in Eq. (3) reduces to unity and thus it is unnecessary to do the time-consuming self-consistent calculation. For other scattering processes, we simplify the term in curly brackets to $1-\cos\theta$ as done in Refs. 10, 13, 17, and 16. Another significant complication is caused by the fact that the matrix element defined in Eq. (4) depends on the initial and final wave vectors $\mathbf{K}$ and $\mathbf{K}'$ also via the $\mathbf{K}$-dependence of the wave functions. This renders futile any attempt to perform analytically at least one of the integrations and also requires the tabulation of all wave functions $\Psi_{\mathbf{K}}^{(\mu)}$. Thus, when dealing with thermal carriers (as in our case) populating only a small region of the 2D $\mathbf{K}$-space, it is reasonable to assume that the wave functions change weakly with $\mathbf{K}$ and to replace $\Psi_{\mathbf{K}}^{(\mu)}$ with the wave function calculated at the zone-center, $\Psi_{\Gamma}^{(\mu)}$ ("Γ-point approximation"). While this approximation has been employed before,[10,13,16] we found at least two cases in which it fails quite dramatically: Considering GaSb and InSb p-channels under biaxial tensile stress, we found that the two lowest-energy subbands, a heavy- and a light-hole subband, cross near the Γ point as the hole sheet density increases. This happens when the symmetry-breaking due to the confining field results in subband minima away from the symmetry-point Γ. This implies that, except in a very small region around the zone center, the Γ-point approximation would mix the heavy- and light-hole wave functions, which would result in a significant and artificial discontinuity of the mobility as a function of the sheet density. A better approximation which we have embraced consists in assuming $\Psi_{\mathbf{K}}^{(\mu)} \approx \Psi_{g}^{(\mu)}$, instead of $\Psi_{\mathbf{K}}^{(\mu)} \approx \Psi_{\Gamma}^{(\mu)}$, where $\Psi_{g}^{(\mu)}$ is the wave function calculated at the extreme point of the μ-th subband (ground-state wave function approximation), in general away from the zone center.

Thorough discussions regarding the physical models for NP,[10,13,17] SR,[25–27] and AL (Ref. 33) scattering have been given in the literature. Thus in the following subsections we will mainly focus on LO- and SO-phonon scattering, and on dielectric screening.

A. Momentum relaxation rate for LO phonon scattering

The relaxation rate due to scattering with LO phonons has been evaluated by adapting to our case the results of Ref. 27 obtaining

$$\frac{1}{\tau_{\mu\nu}(\mathbf{K})} = \frac{e^2\omega_{LO}}{4\pi} \times \frac{1-f(E')}{1-f(E)} \times \left(\frac{1}{\varepsilon_s^\infty} - \frac{1}{\varepsilon_s^0}\right) \times \begin{Bmatrix} n_{LO} \\ 1+n_{LO} \end{Bmatrix} \times \int_0^{2\pi} d\phi \frac{K'}{\frac{\partial E}{\partial K'}} \int_{-\infty}^{\infty} \frac{dq_z}{2\pi} |M_{Q,\mu,\nu,q_z}^{(ex)}|^2 \times (1-\cos\theta), \quad (5)$$

having used the approximated relaxation factor $1-\cos\theta$, θ being the angle between initial and final states $\mathbf{K}$ and $\mathbf{K}'$, and n_{LO} is the Bose function. The matrix element above is expressed as

$$M_{Q,\mu,\nu,q_z}^{(ex)} = \mathcal{F}_{\mu,\nu}(q_z)/\sqrt{Q^2+q_z^2}, \quad (6)$$

with momentum transfer $Q=|\mathbf{K}-\mathbf{K}'|$ and overlap factor

$$F_{\mu\nu}(q_z) = \int_0^\infty \Psi_g^{\dagger(\mu)}(z)\Psi_g^{(\nu)}(z)e^{iq_z z}dz, \quad (7)$$

where the ground-state wave function is indicated by the subscript g.

B. Momentum relaxation rate for SO phonon scattering

When considering the interfacial optical modes arising from the coupling between the insulator optical phonons and the surface plasmons, dealing with the III-V polar channel materials considered here requires an extension of the picture presented in Refs. 29–31, because of the additional presence of the LO phonons in the substrate. Following Refs. 29–31, we proceed in three steps to obtain the scattering strength for the SO phonon scattering. First, we calculate the dispersion of the coupled modes by solving Maxwell's equations at the insulator/substrate boundary (assuming an infinitely thick insulator and no interfacial layers here and in the following) obtaining the following secular equation:

$$\epsilon_{ox}(\omega) + \epsilon_{sub}(\omega,Q) = 0, \quad (8)$$

where ϵ_{ox} is the dielectric function in the insulator given by

$$\epsilon_{ox}(\omega) = \epsilon_{ox}^\infty \frac{(\omega_{LO1}^2-\omega^2)(\omega_{LO2}^2-\omega^2)}{(\omega_{TO1}^2-\omega^2)(\omega_{TO2}^2-\omega^2)}, \quad (9)$$

and ϵ_{sub} is the dielectric function in the substrate

$$\epsilon_{sub}(Q,\omega) = \epsilon_s^\infty \left[1 - \frac{\omega_{p,s}^2(Q)}{\omega^2}\right] + \underbrace{(\epsilon_s^0-\epsilon_s^\infty)\frac{\omega_{TO3}^2}{\omega_{TO3}^2-\omega^2}}_{III-V}, \quad (10)$$

expression in which the last term expressing the ionic dielectric response applies only to III-V compound semiconductors. In Eq. (10) ϵ_s^0 is the static permittivity of substrate, ϵ_{ox}^∞ and ϵ_s^∞ are the optical permittivity for insulator and substrate, respectively, ω_{TO1} and ω_{TO2} are the angular frequencies of the two transverse optical phonon modes of the insulator and the relation between the longitudinal and transverse modes is

given by generalized Lyddane-Sachs-Teller relation as discussed in Ref. 29. Also, ω_{TO3} is the frequency of substrate optical phonons, $\omega_{p,s}=[\Sigma_\nu e^2 n_\nu Q/(2\epsilon_s^\infty m_\nu)]^{1/2}$ is the plasma frequency of the 2D hole gas (2DHG), n_ν and m_ν being the hole density and density-of-state effective mass for subband ν. Equation (8) has multiple solutions. Each one of them represents excitations coupling both the electronic (at the insulator/substrate interface) and the ionic (of the two insulator TO-modes we consider one substrate TO-mode) oscillations.[29] Therefore, in order to consider only excitations able to subtract momentum from the hole gas, we must separate the phonon content from the substrate-plasmon content of each mode. This leads us to the second step, consisting in extracting the relative phonon content for each branch, following Refs. 36 and 37. Finally, in the final step, the scattering strength for each SO mode is calculated and the momentum relaxation rate for SO phonon scattering can be calculated as following:

$$\frac{1}{\tau_{\mu\nu}(\mathbf{K})}=\frac{e^2}{2\pi\hbar}\int_0^{2\pi}d\phi|b_{Q,\omega}|^2|F_{\mu\nu}|^2\frac{K'}{|\partial E/\partial K'|}\times\begin{Bmatrix}n_Q\\n_Q+1\end{Bmatrix}\times\frac{1-f(E_\mu)}{1-f(E_\nu)}\times(1-\cos\theta), \quad (11)$$

where the expressions for scattering strength $b_{Q,\omega}$ and overlap factor $F_{\mu\nu}$ can be found in Ref. 34. In this expression n_Q is the Bose function and K' is determined by

$$Q=|\mathbf{K}-\mathbf{K}'|, \quad (12)$$

$$E_\mu \pm E_\nu=\hbar\omega_Q. \quad (13)$$

These two equations constitute a nonlinear problem which is solved iteratively.[29]

When the collective substrate-plasmon like excitations enter the single-particle continuum in the substrate, plasmons cease to be proper excitation because of their short lifetime leading to a decay into single-particle excitations. (Landau damping). This happens as soon as the plasmon wave vector allows conservation of energy and momentum for decay into a single-particle excitation, that is when

$$\hbar\omega_{LD}^\nu=E^\nu[\mathbf{K}_F+\mathbf{Q}]-E^\nu[\mathbf{K}_F], \quad (14)$$

where $\mathbf{K}_F$ is the carrier wave vector at the Fermi energy at absolute zero and ω_{LD} is the subband-dependent Landau damping frequency. In terms of the complicated valence subband structure, we approximate ω_{LD} by the weighted average

$$\omega_{LD}=\sum_\nu\frac{n_\nu}{n_s}\omega_{LD}^\nu, \quad (15)$$

where the weight-factor n_ν/n_s is the occupation of ν^{th} subband. When $\omega_{p,s}$ is within this region, the physical model of SO phonon scattering coincides with the Wang-Mahan model,[38] in which the coupling between SO phonons and substrate plasmons is effectively suppressed.

A discussion of the dispersion of the interfacial modes, of their phonon and plasmon content, of the scattering strength for each mode and of the effect of Landau damping will be presented in the following section.

C. Dielectric screening

Following the discussion in Refs. 10, 17, and 26, for an arbitrary scattering potential V the screened inter-subband ($\mu\neq\nu$) matrix elements $V_{Q,\mu\nu}$ is given by

$$V_{Q,\mu\nu}=V_{Q,\mu\nu}^{(ex)}-\sum_\lambda\epsilon_{\mu\nu,\lambda\lambda}V_{Q,\lambda\lambda}, \quad (16)$$

where $V_{Q,\mu\nu}^{(ex)}$ is the unscreened scattering matrix element. The diagonal (intrasubband) matrix elements entering the equation above can be obtained by inverting the linear problem

$$\sum_\lambda\epsilon_{\mu\mu,\lambda\lambda}(Q,\omega)V_{Q,\lambda\lambda}=V_{Q,\mu\mu}^{(ex)}, \quad (17)$$

with the dielectric matrix

$$\epsilon_{\mu\nu,\lambda\lambda}(Q,\omega)=\delta_{\mu\nu}\delta_{\lambda\lambda}+\frac{\beta_{\lambda\lambda}}{Q}\Omega_{Q,\mu\nu,\lambda\lambda}, \quad (18)$$

in which Ω is the form factor

$$\Omega_{Q,\mu\nu,\lambda\lambda}=2\int_0^\infty dz\Psi_g^{(\mu)}(z)\Psi_g^{\dagger(\nu)}(z)\times\int_0^\infty dz'\tilde{G}_Q(z,z')\Psi_g^{(\mu)}\times(z')\Psi_g^{\dagger(\nu)}(z'), \quad (19)$$

and again we use the ground-state wave function approximation. The quantity $\tilde{G}$ is the reduced Green's function $\tilde{G}=2QG$, and $\beta_{\lambda\lambda}$ is the 2D screening wave vector. For time-dependent scattering potentials we must employ the dynamic screening wave vector which, in the nondegenerate, high-temperature limit is given by[34,37]

$$\Re[\beta_{\lambda\lambda}^{(2D)}]=\beta_{DH}\frac{\pi^{1/2}}{Q\ell_\lambda}\left\{\Phi\left[\left(\frac{m_\lambda}{2k_BT}\right)^{1/2}\left(\frac{\omega}{Q}+\frac{\hbar Q}{2m_\lambda}\right)\right]-\Phi\left[\left(\frac{m_\lambda}{2k_BT}\right)^{1/2}\left(\frac{\omega}{Q}-\frac{\hbar Q}{2m_\lambda}\right)\right]\right\}, \quad (20)$$

and

$$\Im[\beta_{\lambda\lambda}^{(2D)}]=\beta_{DH}^{(\lambda)}\frac{\pi\hbar\omega}{Q\ell_\lambda k_BT}\times\exp\left(\frac{-m_\lambda\omega^2}{2k_BTQ^2}-\frac{\hbar^2Q^2}{8m_\lambda k_BT}\right)\frac{\sinh[\hbar\omega/(2k_BT)]}{\hbar\omega/(2k_BT)}, \quad (21)$$

where $\beta_{DH}^{(\lambda)}=(e^2n_\lambda/2\epsilon_sk_BT)^{1/2}$ is the 2D Debye–Hückel limit of the dynamic screening wave vector, and $l_\lambda=[2\pi\hbar^2/m_\lambda k_BT]^{1/2}$ is the thermal wavelength of free carriers in the λ^{th} subband, and $\phi(y)=2e^{-y^2}\int_0^y e^{t^2}dt$ is the plasma dispersion function. m_λ is the density-of-state effective mass for the λ^{th} subband.

In static limit ($\omega=0$), only the real part of the screening wave vector is nonzero and it is given by[10,17,26]

$$\beta_{\lambda\lambda}^{(2D)}=\Re[\beta_{\lambda\lambda}^{(2D)}]=\beta_{DH}^{(\lambda)}\frac{2\pi^{1/2}}{Q\ell_\lambda}\Phi\left[\frac{Q\ell_\lambda}{4\pi^{1/2}}\right]. \quad (22)$$

Screening, either dynamic or static, makes the computation of scattering potential more complicated and time-consuming. One way previously widely used to simplify the above screening models is the effective screening model, for

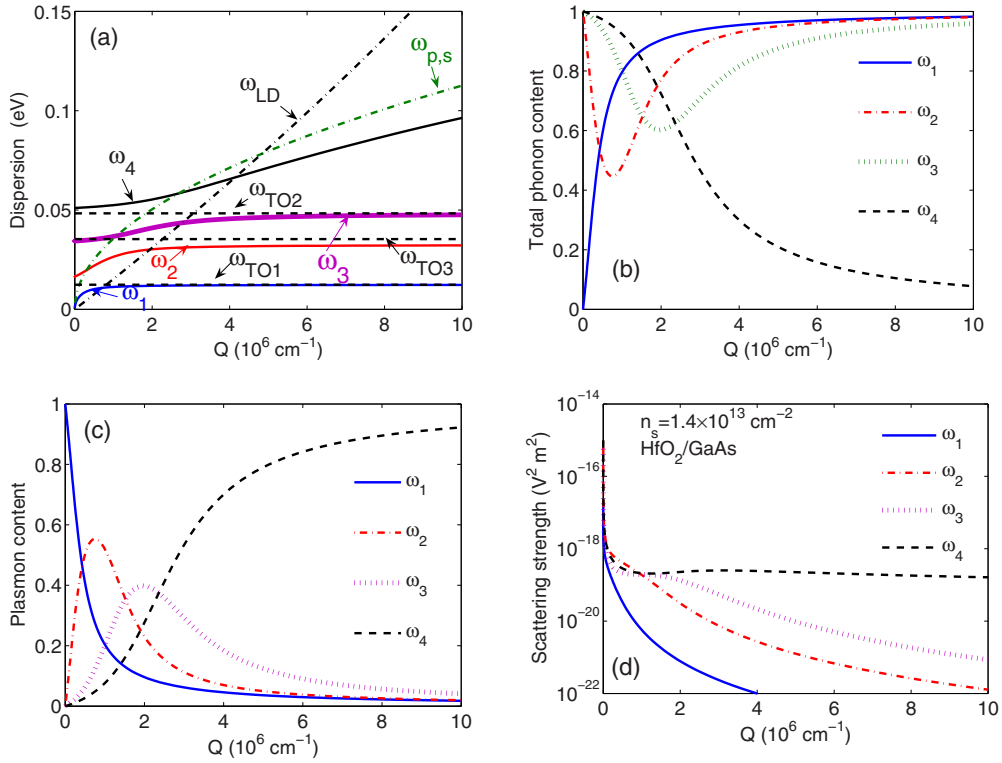

FIG. 1. (Color online) Properties of the SO-modes in a relaxed GaAs p-channel of an MOS system with an HfO_2 insulator: (a) dispersion of the modes (b) total phonon content (TO1+TO2+TO3) (c) and plasmon content of each mode, and (d) hole-SO-modes scattering strength. In (a), ω_{LD} indicates the Landau damping frequency and $\omega_{p,s}$ represents the substrate-plasmon frequency. The frequencies ω_{TO1} and ω_{TO2} label the frequencies for the two insulator optical phonon modes, while ω_{TO3} is the frequency of the substrate optical phonon.

which the complex expression for 2D wave vector is replaced by a scalar given by[38]

$$q_s = \sum_{\lambda} Re[\beta_{\lambda\lambda}^{(2D)}]. \tag{23}$$

The effect of different screening models will be shown in the following section.

IV. DISCUSSIONS AND RESULTS

The structure considered in our simulation is a uniformly doped inversion layer on the (001) interface with an infinitely thick insulator. We assume an infinite barrier-height at the substrate-insulator interface and consider the mobility along the [110] direction at room temperature. A variety of semiconductors (Ge, GaAs, $In_{1-x}Ga_xAs$, GaSb, and InSb) and insulators (SiO_2, HfO_2, ZrO_2, Al_2O_3, and $ZrSiO_4$) are considered. In addition, 2% biaxial stress, either tensile or compressive, is applied to the channel. We have assumed an InP-lattice-matched $In_{1-x}Ga_xAs$ p-channel, so that $x=0.53$ corresponds to the relaxed case, while the values of $x=0.7$ and $x=0.3$ for the mole fraction we have also considered represent biaxial tensile and compressive strained layers, respectively.

Figure 1 shows the calculated results for SO phonon dispersion, phonon content, plasmon content and scattering strength in a relaxed GaAs p-channel inversion layer with HfO_2 at a hole density $n_s=1.4\times10^{13}$ cm^{-2}. The four solutions of Eq. (8) are denoted by ω_1, ω_2, ω_3, and ω_4, in order of increasing frequency at low Q. Landau damping has been ignored in this case. However, the curve labeled ω_{LD} indicates the strong damping region of the substrate plasmons while the curve labeled $\omega_{p,s}$ represents the substrate-plasmon frequency. Strong coupling between interface optical phonons and substrate plasmons can be seen from the mode dispersion, total phonon and plasmon content from Figs. 1(a)–1(c): At small wave vector Q, ω_1 is almost fully substrate-plasmon-type but it approaches the low-energy insulator optical phonon mode ω_{TO1} at large Q. Conversely, at large Q ω_4 is substrate-plasmon-like while at small Q it merges into the high-energy insulator optical phonon mode ω_{TO2}. The branch labeled ω_2 originates from the TO mode ω_{TO1} and converges quickly to the substrate optical phonon mode labeled ω_{TO3}, while its intermediate-Q behavior is mostly substrate-plasmon like. The branch labeled ω_3 has almost the same dispersion as ω_2, but is stars as phonon-like at small Q as ω_{TO3}, ending at ω_{TO2}. The total phonon [Fig. 1(b)] and plasmon [Fig. 1(c)] content also illustrates this strong coupling between substrate plasmons and SO phonons. This coupling enhances the scattering strength, shown in Fig. 1(d). We should recall that the carrier mobility is determined not only by the scattering strength of Fig. 1(d), but also by the energy of each mode. For example, a high-energy ($\hbar\omega > k_BT$) mode will not be emitted very efficiently by low-energy (thermal) carriers and at room temperature its Bose occupation number will be too small to result in any significant number of emission processes either, as discussed in Ref. 29.

Figure 2 illustrates the effect of Landau damping on SO-limited hole mobility for a relaxed GaAs p-channel in both

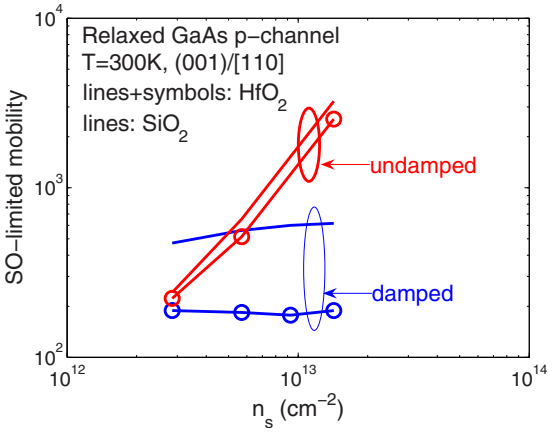

FIG. 2. (Color online) Effect of Landau damping on SO-limited hole mobility in a relaxed GaAs p-channel of an MOS system with an SiO_2 or an HfO_2 gate insulator.

cases of an SiO_2 and an HfO_2 insulator. As we can see, ignoring Landau damping significantly overestimates the SO-limited hole mobility, especially at large hole sheet densities, since in this case the strong dielectric screening due to the substrate plasmons reduces the scattering potential, thus increasing the channel mobility.

In Fig. 3 we compare the LO-limited hole mobility in a relaxed GaAs channel with SiO_2 insulator calculated employing the various dielectric screening models discussed in Sec. III C. One can clearly see that the use of an effective screening parameter underestimates dielectric screening effects, essentially leaving the interaction unscreened and thus yielding a severely underestimated mobility. Somewhat surprisingly, the difference between static screening and screening is almost negligible, mainly because at the large sheet densities we have considered the 2D hole plasma has a frequency large enough to respond to the LO-phonon oscillations. It is thus reasonable to restrict our calculations to the use of a static screening model also in dealing with LO-phonon scattering.

In Fig. 4 we show the various components of the mobility (i.e., limited by a singe scattering process, NP, LO, SO, and SR) in a relaxed GaAs p-channel with SiO_2 and HfO_2 insulators: The interface phonons originating from the high-κ

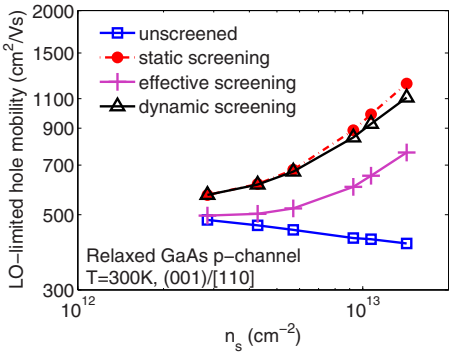

FIG. 3. (Color online) Effect of the various screening models described in the text (effective, static, and dynamic) on the LO-limited hole mobility in a relaxed GaAs p-channel with SiO_2 insulator. The use of the effective-screening model underestimates the hole mobility while static screening shows a modest overestimation of the LO-limited mobility.

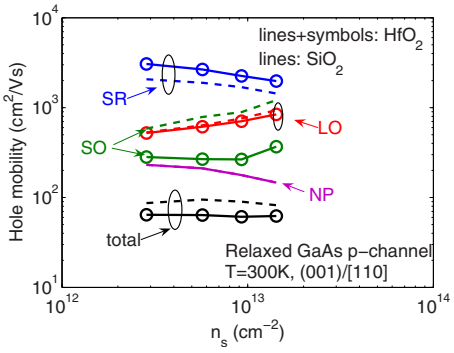

FIG. 4. (Color online) Hole mobility components in a relaxed GaAs p-channel with SiO_2 and HfO_2 insulators.

TO modes exhibit a much stronger scattering strength in the case of HfO_2 than SiO_2, as expected, resulting in a smaller SO-limited hole mobility. However, the presence of a high-κ dielectric improves the SR-limited mobility. This effect stems from the sign of the surface polarization charge induced by the roughness. This charge is proportional to $\epsilon_s - \epsilon_{ox}/\epsilon_s + \epsilon_{ox}$, where ($\epsilon_s$ and ϵ_{ox} are static dielectric constants of the substrate and insulator, respectively. Thus, in the case of SiO_2 the polarization charge increases the amplitude of the SR scattering potential, while in the case of HfO_2 the polarization acts as a screening charge. Consequently, the reduced SR scattering potential compensates for the enhanced SO-scattering potential in high-κ systems.

Figures 5–9 present our results regarding the hole mobility in relaxed, 2% biaxially strained (both compressive and tensile) InSb, GaAs, GaSb, $In_{1-x}Ga_xAs$, and Ge p-channels with HfO_2 and SiO_2 insulators. For the latter, we show results obtained by ignoring or accounting for SO-phonon scattering: Indeed, while the effect of Si/SiO_2 SO-phonon scattering on the electron mobility has been found to be small,[29] we still need to verify that the same is true for the hole mobility in more general situations.

From these figures we can draw the following conclusions: First, the presence of a high-κ insulator degrades the mobility compared with the case of SiO_2, as explained before. Second, the application of stress enhances the mobility with either SiO_2 or HfO_2. In particular, in the case of Ge channels, biaxial tensile strain boosts the mobility by a larger

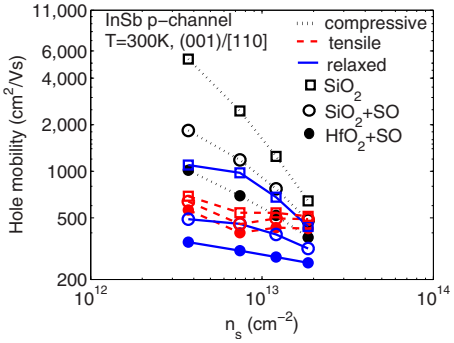

FIG. 5. (Color online) Strain-dependent hole mobility in relaxed (solid line), 2% biaxially compressed (dotted line), and 2% biaxially tensed (dashed line) InSb p-channel with SiO_2 (line) and HfO_2 (symbol) insulators. Stress is applied on the (001) surface.

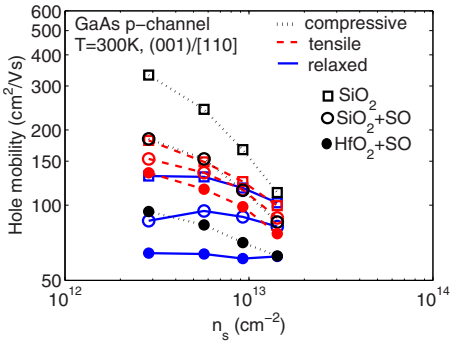

FIG. 6. (Color online) As in Fig. 5, but for GaAs channels.

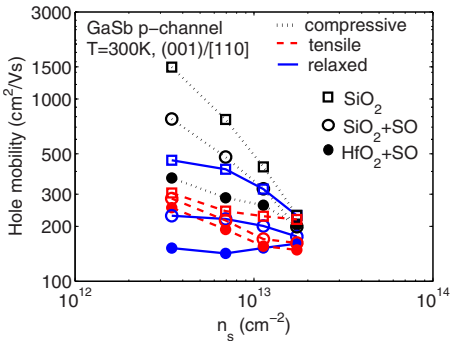

FIG. 7. (Color online) As in Fig. 5, but for GaSb channels.

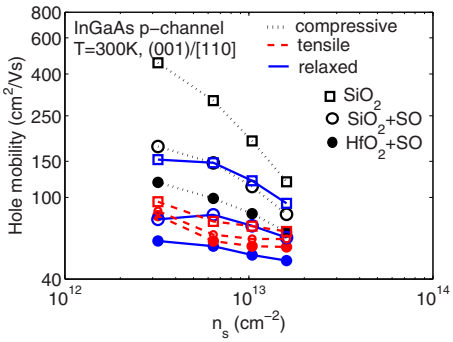

FIG. 8. (Color online) As in Fig. 5, but for $In_{1-x}Ga_xAs$ channels lattice-matched to InP.

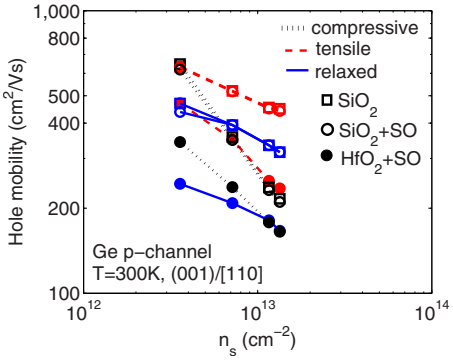

FIG. 9. (Color online) As in Fig. 5, but for Ge channels.

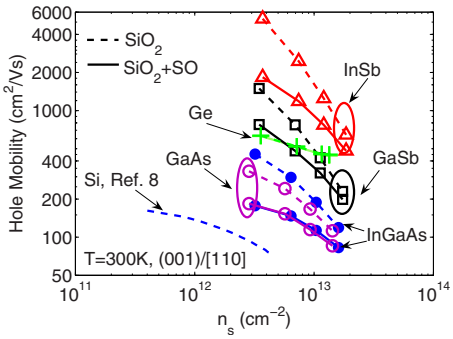

FIG. 10. (Color online) Calculated hole mobility in GaAs, GaSb, InSb, $In_{0.7}Ga_{0.3}As$ p-channels under biaxial compressive strain and Ge channels under biaxial tensile strain with SiO_2 gate insulator including (solid lines) and excluding (dashed lines) the SO phonon scattering. The Si universal curve is from Ref. 8. Biaxial stress is applied on the (001) surface.

extent than compressive strain, the opposite being true for III-V channels. One exception is the case of GaAs channels which exhibit the largest mobility under compressive stress in SiO_2 systems, under tensile stress in HfO_2 systems. Especially noteworthy is the fact that for systems with HfO_2 insulator the mobility seen under the application of biaxial tensile strain is larger than when applying biaxial compressive strain. This might be due to the subband structure dependent Landau damping frequency [Eq. (14)] which renders the biaxial tensile strain case is less sensitive to the high-κ insulator. Third, in relaxed and strained Ge channels with a SiO_2 insulating layer, the effect of SO-phonon scattering on the mobility is consistent with previous observations.[29] However, in III-V p-channels the presence of the substrate LO mode—obviously absent in Ge—results in a slightly different behavior: At low sheet densities the additional interfacial mode originating from the coupling of the substrate LO-phonon with the interfacial plasmons and high-κ modes results in an additional scattering process which, in turn, yields a hole mobility which is very strongly affected by the presence of the high-κ insulator. At higher hole sheet densities, instead, dielectric screening weakens this scattering potential and the difference between the hole mobility in channels with an SiO_2 gate insulator or in channels with a high-κ insulator is reduced. We should also note that, in general, materials with higher hole mobility exhibit a higher sensitivity to SO-phonon scattering than others, which can also be seen from Fig. 10.

In drawing Fig. 10, we have selected for each material the stress condition resulting in the largest mobility enhancement for channels in the presence of an SiO_2 insulator (namely: biaxial compressive strain for III-Vs and biaxial tensile strain for Ge) with (solid lines) and without (dashed lines) SO-phonon scattering. Similarly, Fig. 11 presents the same comparison for HfO_2 systems under biaxial compressive strain is for GaSb, InSb and $In_{1-x}Ga_xAs$) and biaxial tensile strain for GaAs and Ge p-channels. Most notably, while in all cases we see an improvement with respect to the Si universal curve,[8] biaxially compressively strained InSb p-channels yields the best overall result.

In Fig. 12 we show the calculated hole mobility in relaxed Ge channels for a variety of insulators. Among the

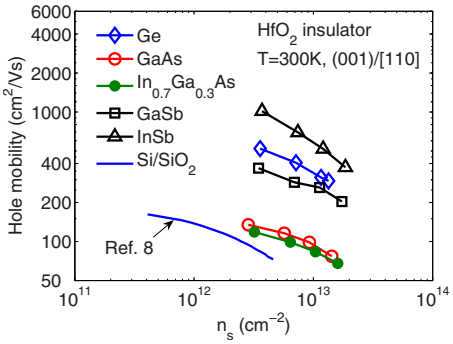

FIG. 11. (Color online) As in Fig. 10 but with HfO_2 insulator.

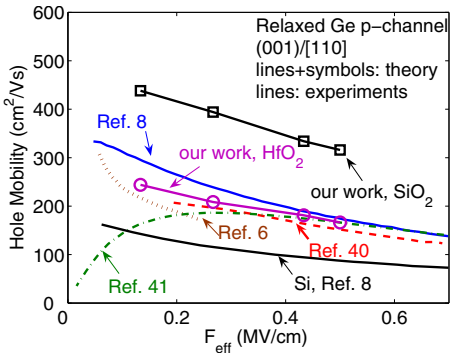

FIG. 13. (Color online) Calculated hole mobility (lines with symbols) on the (001) plane and along the [110] direction in relaxed Ge p-channels compared to experimental data by Shang *et al.* (Ref. 6) (dotted line), Joshi *et al.* (Ref. 8) (solid line), Clavelier *et al.* (Ref. 40) (dashed line), Martens *et al.* (Ref. 41) (dotted-dashed line) and the Si universal curve (solid line) is from Ref. 8. F_{eff} is the effective surface field. Good agreement can be found between experimental data and our simulated results for the HfO_2/Ge system.

insulators we have considered, HfO_2 and ZrO_2 appear to yield the lowest mobility while Al_2O_3 and $ZrSiO_4$ show some promise, which is consistent with the result given by Ref. 29 in the case of the electron mobility.

Finally, we conclude by showing in Fig. 13 a comparison between experimental data and our calculated hole mobility in a relaxed Ge p-channel. Our calculations with a HfO_2 insulator shows good agreement with the experimentally observed values using high-κ insulators,[6,8,39,40] while results with a SiO_2 insulator yield a much larger mobility for the reasons explained before.

V. CONCLUSIONS

In this paper we have presented a comprehensive theoretical study of the hole mobility p-channels of both relaxed and biaxially strained Ge and III-V MOS systems with a variety of insulators. Our model is based on a six-band $\mathbf{k}\cdot\mathbf{p}$/Poisson self-consistent valence subband structure and physically accurate models to handle nonpolar scattering with acoustic and optical phonons, statically-screened surface roughness scattering, Fröhlich scattering with substrate LO phonons, scattering with high κ-induced surface-optical modes, and alloy scattering. Our main result consists in the observation that both Ge and III-V materials exhibit a hole mobility larger than the universal relaxed-Si value with either SiO_2 or HfO_2 insulators. In addition, biaxially compressively strained InSb can provide largest hole mobility, but also $In_{0.7}Ga_{0.3}As$ lattice-matched to InP (and so biaxially compressively stressed as well) exhibits a promising mobility enhancement. Finally, we have shown that the presence of high-insulators can depress the hole mobility. On the other hand, we should keep in mind our initial observations regarding the weak connection we should expect between low-field mobility and performance, as well as the fact that the strength of scattering with interfacial SO modes decreases at larger carrier energy. Thus, the effect of high-insulators on the performance of the devices at high-bias may not be as deleterious as it appears when focusing only on the low-field mobility. Similar considerations have already been made in Ref. 41, where the simulated on-performance of high–based short-channel Si MOSFETs was found to be essentially unaffected by the presence of the high-k insulator

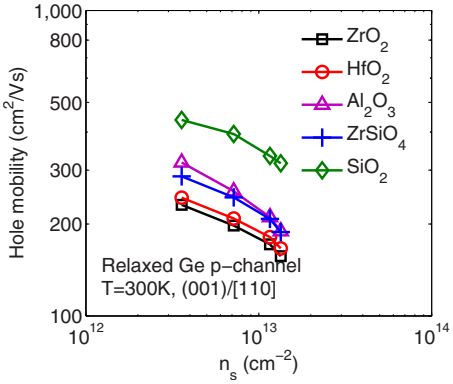

FIG. 12. (Color online) Hole mobility in relaxed Ge p-channels with a variety of gate insulators. Not surprisingly, our results show that high-κ dielectrics affect negatively the hole mobility, compared with channels with an SiO_2 insulator, due to the effect of remote phonons. In addition, ZrO_2 and HfO_2 degrade hole mobility more than Al_2O_3 and $ZrSiO_4$.

ACKNOWLEDGMENTS

This work has been funded by GRC and MARCO MSD.

[1] A. Cros, K. Romanjek, D. Fleury, S. Harrison, R. Cerutti, P. Coronel, B. Dumont, A. Pouydebasque, R. Wacquez, B. Duriez, *et al.*, Tech. Dig. - Int. Electron Devices Meet. **2006**, 663.
[2] V. Barral, T. Poiroux, J. Saint-Martin, D. Munteanu, J.-L. Autran, and S. Deleonibus, IEEE Trans. Electron Devices **56**, 408 (2009).
[3] V. Barral, T. Poiroux, D. Munteanu, J.-L. Autran, and S. Deleonibus, IEEE Trans. Electron Devices **56**, 420 (2009).
[4] R. Chau, Solid State Technol. **51**, 30 (2008).
[5] M. L. Lee, C. W. Leitz, Z. Cheng, A. J. Pitera, T. Langdo, M. T. Currie, G. Taraschi, E. A. Fitzgerald, and D. A. Antoniadis, Appl. Phys. Lett. **79**, 3344 (2001).
[6] H. Shang, H. Okorn-Schimdt, J. Ott, P. Kozlowski, S. Steen, E. C. Jones, H.-S. P. Wong, and W. Hanesch, IEEE Electron Device Lett. **24**, 242 (2003).
[7] A. Ritenour, S. Yu, M. L. Lee, N. Lu, W. Bai, A. Pitera, E. A. Fitzgerald, D. L. Kwong, and D. A. Antoniadis, Tech. Dig. - Int. Electron Devices Meet. **2003**, 18.2.1.
[8] S. Joshi, C. Krug, D. Heh, H. J. Na, H. R. Harris, J. W. Oh, P. D. Kirsch, P. Majhi, B. H. Lee, H. H. Tseng, R. Jammy, J. C. Lee, and S. K. Banerjee, IEEE Trans. Elec. Device Lett. **28**, 308 (2007).
[9] M. Passlack, R. Droopad, I. Thayne, and A. Asenov, Solid State Technol. **51**, 26 (2008).
[10] M. V. Fischetti, Z. Ren, P. M. Solomon, M. Yang, and K. Rim, J. Appl. Phys. **94**, 1079 (2003).
[11] R. Oberhuber, G. Zandler, and P. Vogl, Phys. Rev. B **58**, 9941 (1998).

[12]C. Moglestue, J. Appl. Phys. **59**, 3175 (1986).
[13]E. X. Wang, P. Matagne, L. Shifren, B. Obradovic, R. Kotlyar, S. Cea, M. Stettler, and M. D. Giles, IEEE Trans. Electron Devices **53**, 1840 (2006).
[14]Y. Sun, S. E. Thompson, and T. Nishida, J. Appl. Phys. **101**, 104503 (2007).
[15]T. O'Regan and M. V. Fischetti, Jpn. J. Appl. Phys., Part 1 **46**, 3265 (2007).
[16]A. T. Pham, C. Jungemann, and B. Meinerzhagen, IEEE Trans. Electron Devices **54**, 2174 (2007).
[17]Y. Zhang, M. V. Fischetti, B. Sorée, W. Magnus, M. Heyns, and M. Meuris, J. Appl. Phys. **106**, 083704 (2009).
[18]M. V. Fischetti, T. O'Regan, S. Narayanan, C. Sachs, S. Jin, J. Kim, and Y. Zhang, IEEE Trans. Electron Devices **54**, 2116 (2007).
[19]Y. Zhang, J. Kim, and M. V. Fischetti, J. Comput. Electron. **7**, 176 (2008).
[20]E. Bangert and G. Landwehr, Surf. Sci. **58**, 138 (1976).
[21]A. T. Pham, C. Jungemann, and B. Meinerzhagen, J. Comput. Electron. **7**, 99 (2008).
[22]J. M. Luttinger and W. Kohn, Phys. Rev. **97**, 869 (1955).
[23]J. M. Luttinger, Phys. Rev. **102**, 1030 (1956).
[24]T. Ando, J. Phys. Soc. Jpn. **43**, 1616 (1977).
[25]T. Ando, A. B. Fowler, and F. Stern, Rev. Mod. Phys. **54**, 437 (1982).
[26]S. Jin, M. V. Fischetti, and T. Tang, IEEE Trans. Electron Devices **54**, 2191 (2007).
[27]R. W. Kelsall, R. I. Taylor, A. C. G. Wood, and R. A. Abram, Semicond. Sci. Technol. **5**, 877 (1990).
[28]Y. Zhang and M. V. Fischetti, International Workshop of Computational Electronics **7**, 176 (2009).
[29]M. V. Fischetti, D. A. Neumayer, and E. A. Cartier, J. Appl. Phys. **90**, 4587 (2001).
[30]M. V. Fischetti, J. Appl. Phys. **89**, 1232 (2001).
[31]M. V. Fischetti and S. E. Laux, J. Appl. Phys. **89**, 1205 (2001).
[32]R. W. Kelsall and R. A. Abram, Semicond. Sci. Technol. **7**, B312 (1992).
[33]M. V. Fischetti and S. E. Laux, J. Appl. Phys. **80**, 2234 (1996).
[34]M. V. Fischetti and S. E. Laux, Phys. Rev. B **48**, 2244 (1993).
[35]I. Vurgaftman, J. R. Meyer, and L. R. Ram-Mohan, J. Appl. Phys. **89**, 5815 (2001).
[36]A. L. Fetter and J. D. Walecka, *Theoretical Mechanics of Particles and Continua* (Dover, New York, 2003).
[37]S. Q. Wang and G. D. Mahan, Phys. Rev. B **6**, 4517 (1972).
[38]F. Riddoch and B. Ridley, J. Phys. C **16**, 6971 (1983).
[39]L. Clavelier, J. F. Damlencourt, C. L. Royer, B. Vincent, Y. Morand, Y. Campidelli, J. M. Hartmann, E. Martinez, Q. T. Nguyen, S. Cristoloveanu *et al.*, Proceedings of the IEEE International SOI Conference, 2007, p. 19.
[40]K. Martens, http://sites.google.com/site/phdkoenmartens/Home/phd-thesis (2009).
[41]M. V. Fischetti, S. Jin, T. w. Tang, P. Asbeck, Y. Taur, S. Laux, M. Rodwell, and N. Sano, J. Comput. Electron. **8**, 60 (2009).